Distinguishing environmental effects on binary black hole gravitational waveforms

Cole, P.S.; Bertone, G.; Coogan, A.; Gaggero, D.; Karydas, T.; Kavanagh, B.J.; Spieksma, T.F.M.; Tomaselli, G.M.

DOI
10.1038/s41550-023-01990-2

Publication date
2023

Document Version
Final published version

Published in
Nature Astronomy

nature astronomy

Article

https://doi.org/10.1038/s41550-023-01990-2

Distinguishing environmental effects on binary black hole gravitational waveforms

Received: 10 November 2022

Accepted: 3 May 2023

Published online: 5 June 2023

Check for updates

Philippa S. Cole[1] ✉, Gianfranco Bertone[1], Adam Coogan[2,3,4], Daniele Gaggero[5,6], Theophanes Karydas[1], Bradley J. Kavanagh[7], Thomas F. M. Spieksma[1,8] & Giovanni Maria Tomaselli[1]

Future gravitational wave interferometers such as the Laser Interferometer Space Antenna, Taiji, DECi-hertz Interferometer Gravitational wave Observatory and TianQin will enable precision studies of the environment surrounding black holes. These detectors will probe the millihertz frequency range, as yet unexplored by current gravitational wave detectors. Furthermore, sources will remain in band for durations of up to years, meaning that the inspiral phase of the gravitational wave signal, which can be affected by the environment, will be observable. In this paper, we study intermediate and extreme mass ratio binary black hole inspirals, and consider three possible environments surrounding the primary black hole: accretion disks, dark matter spikes and clouds of ultra-light scalar fields, also known as gravitational atoms. We present a Bayesian analysis of the detectability and measurability of these three environments. Focusing for concreteness on the case of a detection with LISA, we show that the characteristic imprint they leave on the gravitational waveform would allow us to identify the environment that generated the signal and to accurately reconstruct its model parameters.

The next generation of gravitational wave (GW) detectors are expected to come online in the 2030s. Those set to explore the milli- and deci-hertz regimes, such as the Laser Interferometer Space Antenna (LISA)[1], Taiji[2], DECi-hertz Interferometer Gravitational wave Observatory (DECIGO)[3] and TianQin[4], will open a new window for GW discoveries. They will have a much lower frequency range than the current Laser Interferometer Gravitational-Wave Observatory[5], Virgo[6] and Kamioka Gravitational Wave Detector[7] detectors. For example, LISA is expected to be sensitive in the range of 10^{-4}–1 Hz, meaning that black hole (BH) binaries with much larger chirp masses will be detectable. Moreover, these sources will stay in band for long durations, up to weeks, months or years in some cases, especially for intermediate mass ratio inspirals (IMRIs) and extreme mass ratio inspirals (EMRIs), which take longer to inspiral than more equal-mass binaries. Observations of IMRIs and EMRIs provide a unique opportunity to learn about the environments of the binaries[8–10]. This is because not only will the binaries stay in the sensitive range of the detector for a considerable amount of time, allowing the imprints of environmental effects to accumulate in the gravitational waveform, but also the environment of the central BH is more robust to disruptions by a much lighter companion object[11].

In this Article, we compare environmental effects on intermediate mass ratio binaries in the millihertz band in three different scenarios, namely accretion disks[12–18], cold dark matter (CDM) spikes[19–27] and clouds of ultra-light scalar fields[28–35]. We are predominantly interested in learning about the nature of dark matter (DM) from the gravitational waveform, and hence our focus is on the modelling of CDM density

[1]Gravitation Astroparticle Physics Amsterdam (GRAPPA), Institute for Theoretical Physics Amsterdam and Delta Institute for Theoretical Physics, University of Amsterdam, Amsterdam, the Netherlands. [2]Ciela – Computation and Astrophysical Data Analysis Institute, Montreal, Quebec, Canada. [3]Département de Physique, Université de Montréal, Montreal, Quebec, Canada. [4]Mila – Quebec AI Institute, Montreal, Quebec, Canada. [5]INFN Sezione di Pisa, Polo Fibonacci, Pisa, Italy. [6]Instituto de Física Corpuscular, Universidad de Valencia and CSIC, Paterna, Spain. [7]Instituto de Física de Cantabria, UC-CSIC, Santander, Spain. [8]Niels Bohr International Academy, Niels Bohr Institute, Copenhagen, Denmark. ✉e-mail: p.s.cole@uva.nl

https://doi.org/10.1038/s41550-023-01990-2

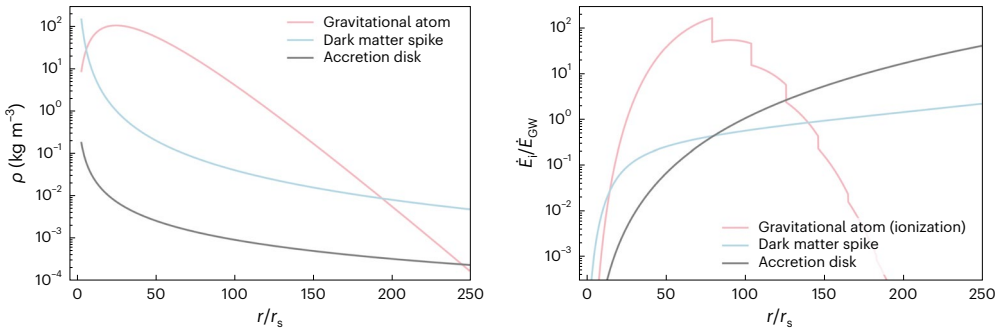

Fig. 1 | Density profiles of and energy losses due to environments. Left: Initial density profiles of environments around a $10^5\,M_\odot$ BH. Right: Energy losses due to environment normalized by the energy losses due to GWs.

spikes around BHs and clouds of ultra-light scalar fields produced by superradiance—a system that is otherwise known as a gravitational atom. However, accretion disks can act on the waveform in the same way as these dark spikes and clouds, so it is vital to determine whether there is a chance of confusion between DM and baryonic effects.

Modelling the environments

We study three possible environments for IMRIs and EMRIs that may have an observable effect on the gravitational waveform: accretion disks, DM spikes and clouds of ultra-light scalar fields, also known as gravitational atoms. These environments can be characterized by their density profiles around the central BH with mass m_1 (Fig. 1, left panel).

Cold collisionless DM

We model the initial density profile of the CDM spike with a power law in r, the radial distance from the central black hole:

$$\rho_{\rm CDM}(r) = \rho_6\left(\frac{r_6}{r}\right)^{\gamma_{\rm s}}, \tag{1}$$

where ρ_6 is the density of the spike at a reference distance of $r_6 = 10^{-6}$ pc from the central BH and $\gamma_{\rm s}$ is the slope of the spike. For spike formation from the adiabatic growth of an intermediate mass black hole at the centre of a DM halo with an initial slope of $\gamma_{\rm i}$, the final slope of the spike will be $\gamma_{\rm s} = (9 - 2\gamma_{\rm i})/(4 - \gamma_{\rm i})$ (ref. 19). For typical values of $\gamma_{\rm i} \in [0, 2]$, this gives $\gamma_{\rm s} \in [2.25, 2.5]$, with a value of $\gamma_{\rm s} = 7/3$ for an initial Navarro–Frenk–White profile, which we assume here.

Gravitational atom

The ultra-light boson cloud surrounding the central BH is assumed to be in a pure $|n\ell m\rangle$ eigenstate, with wavefunction $\psi(t, \mathbf{r}) = R_{n\ell}(r)Y_{\ell m}(\theta, \phi)e^{-i(\omega_{n\ell m} - \mu)t}$, where $\boldsymbol{r}$ is the position vector with respect to the central BH, t is time, $Y_{\ell m}$ are spherical harmonics and $R_{n\ell}(r)$ are the hydrogenic radial functions as laid out explicitly in ref. 34. Additionally, ψ is related to the scalar field Φ via $\Phi = \psi e^{-i\mu t}/\sqrt{2\mu}$, where μ is the mass of the scalar field. This model is valid under the assumption of $\alpha/\ell \ll 1$, where $\alpha \equiv Gm_1\mu$ is the so-called gravitational fine structure constant, in which case the cloud is mostly non-relativistic. The mass density can then be defined as

$$\rho(\mathbf{r}) = M_{\rm c}|\psi(\mathbf{r})|^2, \tag{2}$$

where $M_{\rm c}$ is the total mass of the cloud. If Φ is a real rather than a complex field, ψ has to be replaced with $2\Re[\psi]$ in its relation to Φ and ρ. The value of $M_{\rm c}$ is determined by the mass and spin of the BH before the superradiant instability formed the cloud, and can reach a maximum of about 10% of the central BH mass. We will consider $M_{\rm c}$ as an independent parameter because other processes, such as the decay of the cloud into GWs[36], can change its value.

Accretion disk

We model a locally isothermal disk, which is equivalent to a locally constant speed of sound and therefore a locally constant Mach number $M = r/h$, where h is the scale height of the disk. Given that we are interested in very dense environments in order for environmental effects to cause a substantial dephasing, we will focus on thin disks such that $M \gg 1$. In terms of the surface density of the disk, we use the same parameterization as in ref. 15 (a compromise between the seminal α- and β-disk prescriptions of ref. 37) so as to be in the regime where analytical expressions for gas torques in accretion disks have been calibrated with numerical simulations ('Energy losses' section). The surface density is described as a static power-law profile

$$\Sigma(r) = \Sigma_0\left(\frac{r}{3r_{\rm S}}\right)^{-1/2}, \tag{3}$$

where Σ_0 is the surface density normalization, $r_{\rm S}$ is the Schwarzschild radius of the central BH and the slope has been fixed. See ref. 16 for the case of a varying slope. Finally, we estimate the volume density of the disk for the purpose of comparison with the other environments in the left-hand panel of Fig. 1 with $\rho(r) = \Sigma(r)/2h$.

Energy losses

The evolution of the binary's inspiral depends on the rate of energy loss of the system. We assume that the companion m_2 moves slowly inwards on quasi-circular orbits. Low eccentricity is expected for IMRIs and EMRIs in accretion disks[38], and is partially justified for the case of the dark dress due to dynamical friction (DF) circularizing the binary's orbit[39]. The state-of-the-art calculations for feedback in the dark dress[24] and ionization[34,35] in the gravitational atom scenarios currently only account for circular orbits. We plan to include eccentricity in these formalisms in future analyses. We also assume that energy balance is satisfied with $\dot{E}_{\rm orb} = -\dot{E}_{\rm GW} - \dot{E}_{\rm env}$, where we use the Keplerian expression for the orbital energy $E_{\rm orb} = -Gm_1m_2/(2r)$ and model the GW energy losses at Newtonian order. We model the energy losses induced by the environment $\dot{E}_{\rm env}$ as a linear combination of the relevant effects for each system, including DF, ionization, torques and accretion onto the companion object, all of which are described in detail in the Supplementary Information and briefly summarized in this section.

The relative importance of the environmental effects with respect to the energy radiated away owing to GWs is shown in Fig. 1 (right panel), where we plot $\dot{E}_{\rm env}/\dot{E}_{\rm GW}$ as a function of the separation of the binary in units of Schwarzschild radii for the benchmark parameters given in 'Benchmark system' section. In each case, we work under the assumption of a small mass ratio $q = m_2/m_1 < 10^{-2.5}$ such that the environment is not destroyed within the first few close encounters of the binary, and also so that the companion object can be treated as a point mass without an environment of its own.

https://doi.org/10.1038/s41550-023-01990-2

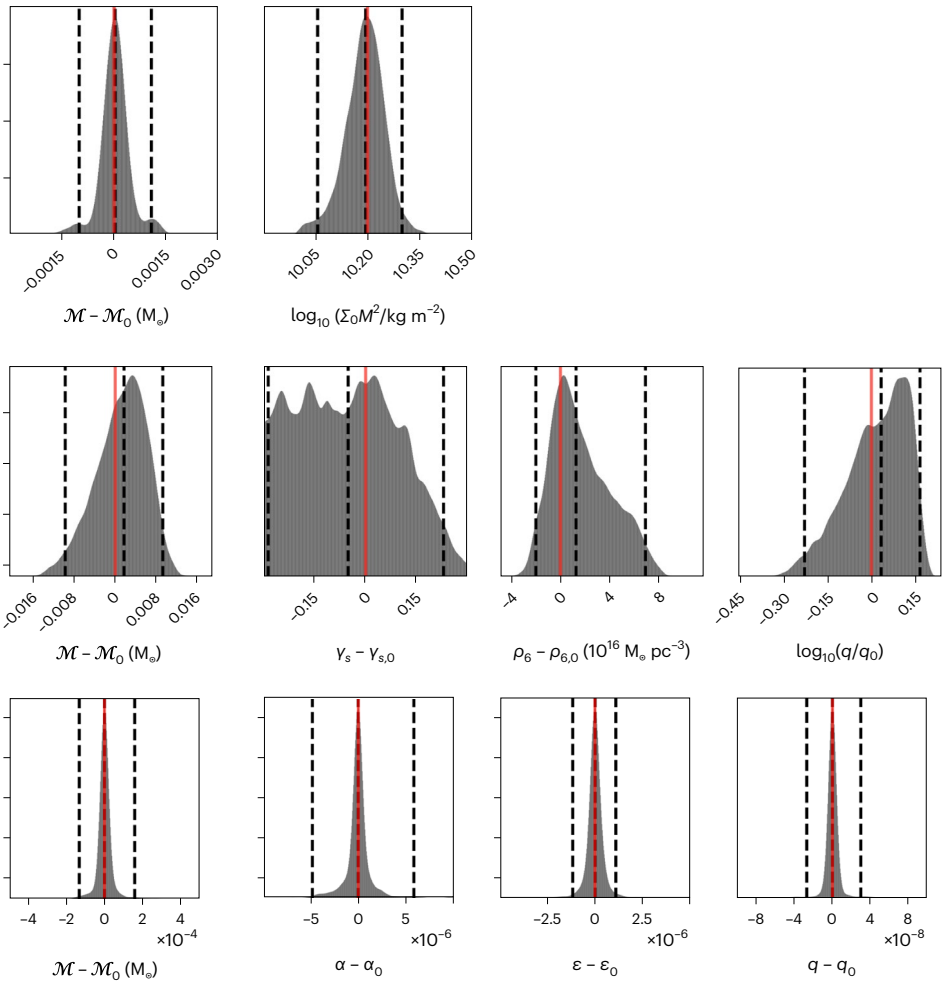

Fig. 2 | Parameter estimation using the correct environmental template. One-dimensional posterior distributions for intrinsic and environmental parameters of an accretion disk (top row), dark matter spike (middle row) and gravitational atom (bottom row) signals with 1 year duration using the correct template in each case. The red vertical lines show the true values of the parameters for each signal, the outermost black dashed vertical lines show the 95% credible intervals of the posteriors and the central dashed black line is the median value of the posteriors. Note that we use the notation $\epsilon = M_c/m_1$ for brevity.

Cold collisionless DM

We model the effects of a DM spike, including feedback on the spike itself, following refs. 24,25. In this framework, the effect of accretion is sub-dominant, so the energy losses are solely due to DF, $\dot{E}_{\rm env} = \dot{E}_{\rm DF}$, which takes the form (appendix L in ref. 40)

$$\dot{E}_{\rm DF} = \frac{4\pi G^2 m_2^2 \rho_{\rm CDM}(r,t)\xi(v)\log\Lambda}{v}, \tag{4}$$

where v is the orbital velocity, $\xi(v)$ is the fraction of DM particles moving more slowly than v and $\log\Lambda$ is the Coulomb logarithm, which encodes information about the minimum and maximum impact parameters relevant for DF. We assume that the DM velocity distribution is isotropic.

Gravitational atom

The case of the gravitational atom is modelled similarly to that in ref. 34. The orbits are assumed to lie on the equatorial plane defined by the spin of the central BH and of the cloud, and we choose for the companion to be co-rotating with the cloud. Besides GW emissions, two effects are taken into account for the binary evolution: the 'ionization' of the cloud due to the gravitational perturbation of the secondary, and the accretion of the cloud by the smaller BH moving through it so we have $\dot{E}_{\rm env} = \dot{E}_{\rm ion} + \dot{E}_{\rm acc}$. Note that the energy is not conserved because accretion is a dissipative process. The balance of angular momentum, however, can be written in a similar form, where accretion contributes as an additional 'force' (see equation (2) in the Supplementary Information).

Accretion disk

In the case of accretion disks, the dominant cause of dephasing for compact binaries arises from gas torques (Supplementary Information). In analogy with so-called type I planet migration, we write the total net torque on the secondary BH, with mass much smaller than the primary BH, co-planar with, and fully embedded in, an accretion disk, as[12,15,41]

$$T_0 = -\Sigma(r) r^4 \Omega^2 q^2 M^2, \tag{5}$$

where M is the Mach number of the disk, $\Sigma(r)$ is the surface density of the (unperturbed) disk, Ω is the orbital angular velocity and q is the mass ratio (see the discussion in the Supplementary Information). Note that the negative sign makes torques act in the same direction as DF, so they lead to a faster inspiral with respect to the vacuum case. We can write the energy losses due to gas torques T_0 in a differentially rotating accretion disk as

$$\dot{E}_{\rm torque} = \frac{G^{\frac{1}{2}} T_0 m_1}{4 r^{\frac{3}{2}} (m_1 + m_2)^{\frac{1}{2}}}. \tag{6}$$

https://doi.org/10.1038/s41550-023-01990-2

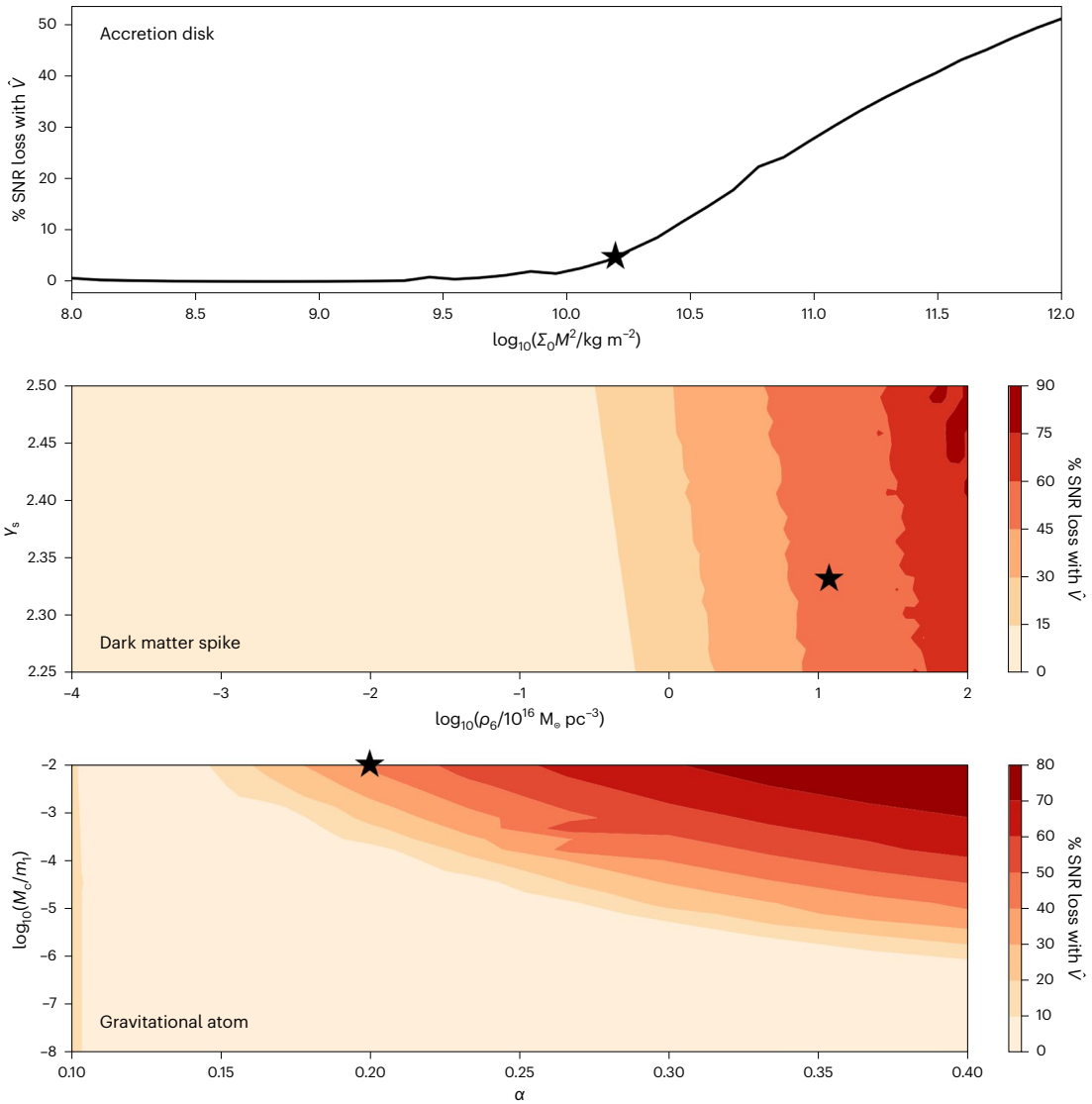

Fig. 3 | SNR losses as a function of the environmental parameters. SNR loss with respect to best-fit vacuum $\hat{V}$ system for accretion disk (top), dark matter spike (middle) and gravitational atom (bottom) signals with 1 year duration. Black stars indicate the benchmark parameters in each case.

Parameter inference to distinguish between environments

Benchmark system

We study a BH binary system with masses $m_1 = 10^5\ \mathrm{M_\odot}$ and $m_2 = 10\ \mathrm{M_\odot}$ and hence chirp mass $\mathcal{M}_{c,0} \approx 398\ \mathrm{M_\odot}$. The expected merger rates for these masses have been predicted to be on the order of 100–1,000 (ref. 42), albeit with large uncertainties, and we defer the prediction of a merger rate for each specific environment to future work. We choose this m_1 because there are plausible formation scenarios for all three environments around a central object of this mass (see, for example, ref. 19 for cold, collisionless DM, ref. 43 for accretion disks and refs. 30,44 for gravitational atoms). Furthermore, the vacuum innermost stable circular orbit (ISCO) frequency of this system, $f_{\mathrm{ISCO}} = 0.044$ Hz, lies close to the bucket of the LISA noise curve, meaning that inspirals will take place in a frequency range of high detector sensitivity. Lastly, we choose a small mass ratio, $q = m_2/m_1 = 10^{-4}$, such that the environments are not disrupted substantially by the companion object, and hence various assumptions that rely on this when calculating the energy losses hold.

The benchmark parameters we choose for each environment are as follows: For the dark dress, $\rho_6 = 1.17 \times 10^{17}\ \mathrm{M_\odot\ pc^{-3}}$ and $\gamma_s = 7/3$ (ref. 19), for the accretion disk, $\Sigma_0 M^2 = 1.5 \times 10^{10}\ \mathrm{kg\ m^{-2}}$, and for the gravitational atom, $\alpha = 0.2$ and $M_c/m_1 = 0.01$ (refs. 34,35). The value of $\Sigma_0 M^2$ we choose for the accretion disk is unrealistically high in that it implies an accretion rate around 100 times larger than the Eddington accretion rate if the β-disk prescription of ref. 37 is used (also see, for example, ref. 45 for recent observations), but since we are mainly concerned with confusing a DM spike for an accretion disk, we want to show that, when the effect of the dephasing is comparable, we can still distinguish between the environments. The signal-to-noise ratio (SNR) loss with respect to the best-fit vacuum signal is non-negligible ('Distinguishing between environments' section), providing a conservative comparison with the dark dress and gravitational atom. Dark dress and gravitational atom signals would be even more readily differentiable from accretion disks if we restricted accretion disk templates to only allow for lower and more realistic values of $\Sigma_0 M^2$, which would imply lower accretion rates. Note that increasing any one of these parameters at a time increases the amount of dephasing with respect to the vacuum system ('Distinguishing between environments' section and Supplementary Information). The same is true of increasing the duration of the signal (Supplementary Information).

Table 1 | Prior ranges used for parameter estimation carried out using nested sampling. All posteriors are contained within the priors except for γ_s

	$\mathcal{M}_c$	$\log_{10}(q)$	$\boldsymbol{\theta}_{\rm env}$
Dark dress	$\mathcal{M}_{c,0} \pm 0.01\,M_\odot$	$\mathcal{U}(-5,-2.5)$	$\rho_6 = \mathcal{U}(0,10^{22})\,M_\odot\,{\rm pc}^{-3}$
			$\gamma_s = \mathcal{U}(2,2.5)$
Accretion disk	$\mathcal{M}_{c,0} \pm 0.005\,M_\odot$	N/A	$\Sigma_0 M^2 = 10^{\mathcal{U}(8,14)}\,{\rm kg\,m}^{-2}$
Gravitational atom	$\mathcal{M}_{c,0} \pm 0.01\,M_\odot$	$\mathcal{U}(-5,-2.5)$	$\alpha = \mathcal{U}(0.1,0.4)$
			$M_c/m_1 = 10^{\mathcal{U}(-8,-2)}$

Parameter estimation with correct model

Firstly, we demonstrate that we can reconstruct the parameters of each environment from the gravitational waveform of a detected 1-year-duration signal, if matched filtering using a template bank with the correct parameters is used. We use the final year of the signal pre-merger, and fix the luminosity distance at $d_L = 3.3$ Gpc such that the SNR is 15 for each system. This corresponds to a redshift of approximately 0.6. We run parameter estimation using the nested sampling[46–48] code `dynesty`[49], with the log likelihood given by the match integral between the sky- and polarization-angle averaged signal $d(t)$ and template $h(t)$, maximized over the extrinsic parameters (Supplementary Information).

The posteriors for the intrinsic and environmental parameters are shown in Fig. 2 for the dark dress, accretion disk and gravitational atom. All posteriors are smoothed with a 2% Gaussian kernel, and the prior ranges are given in Table 1. The minimum values of ρ_6 for the dark dress and M_c for the gravitational atom allow for zero-density environments, while we use a larger minimum prior on $\Sigma_0 M^2$ for the accretion disk since there is no support in the posterior for lower values when trying to mimic more extreme systems. The maximum values for these parameters all allow for the accumulated dephasing to become large enough to mimic the fiducial, most extreme, gravitational atom system. The prior on γ_s corresponds to the physically expected values from adiabatic growth of a DM spike around an intermediate mass black hole[19], while the prior on α ensures that a cloud could have grown via superradiance around BHs with the masses of interest. The priors for the chirp mass $\mathcal{M}_c$ are narrow because the full prior volume drops out of the Bayes factor calculation when comparing models. The red lines show the true values of the signal, while the vertical dashed lines show the 95% (that is, 2σ) credible intervals. Intrinsic and environmental parameters are measured to excellent precision for all three environments with the exception of γ_s, for which longer duration signals are required (Supplementary Information). The precision of the measurements in the case of the gravitational atom is better than the systematic uncertainties in the waveform model. This shows that there is very little degeneracy between these parameters and prospects for measuring them from data are very hopeful, since orders of magnitude degradation in precision of the measurement would still lead to confident parameter inferences. Based on these extremely narrow posteriors for 1 year's worth of data, we also show the posterior distributions for 1 month's worth of data in the Supplementary Information, where all parameters are still very accurately measured with a degradation of the 95% credible intervals by approximately an order of magnitude. Note that the mass ratio q cannot be individually measured in the case of the accretion disk, because it appears in combination with $\Sigma_0 M^2$ in the dephasing contribution. This also explains the slightly better precision in the chirp mass measurement for the accretion disk over the dark dress, because we have fixed the mass ratio to its true value of 10^{-4}.

Having shown that we can precisely measure the parameters of each system using the correct model in each case, we now test whether it is possible to fit each system with an incorrect model.

Distinguishing between environments

Current GW template banks use only vacuum waveforms, so we first demonstrate that we can distinguish each environmental signal from the corresponding best-fit vacuum case. We diagnose the regions of the parameter space for each system where it might be possible to fit an environmental signal with a biased vacuum template by calculating the SNR lost between the signal and template waveforms. As a rule of thumb, we expect SNR losses of more than 30% to compromise the ability to detect the signal with an incorrect template, and systems that incur small SNR losses we expect to lead instead to biased parameter estimation. The SNR loss results are shown in Fig. 3 for best-fit vacuum templates.

For the dark dress, a system with the well-motivated benchmark parameters that we measured in the previous section incurs SNR losses of order 50%. For the accretion disk, the SNR lost between the signal and the best-fit vacuum is 5%, which provides a conservative comparison with the dark dress and the gravitational atom, since more realistic and lower values of $\Sigma_0 M^2$ with lower SNR loss would be more easily distinguishable. For the gravitational atom, a system with $\alpha = 0.2$ and a conservative cloud mass of 1% of the BH mass leads to an SNR loss of ~40%. Larger values of α lead to larger SNR loss, while decreasing the mass of the cloud leads to smaller SNR loss as this approaches the vacuum regime.

To demonstrate that these SNR losses produce biased parameter inferences when using the incorrect template for systems with high SNR loss, we run parameter estimation for the benchmark systems using nested sampling with a vacuum template bank. The posteriors for the chirp mass, which is the only free intrinsic parameter for a GR-in-vacuum waveform in our setup, are shown in Fig. 4. When a vacuum template is used, the chirp mass for the accretion disk system is shifted from its true value by $3.3 \times 10^{-3}\,M_\odot$, for the dark dress by $0.49\,M_\odot$ and for the gravitational atom by $5.4\,M_\odot$. This is explained by a larger chirp mass mimicking the speed-up of the inspiral due to the environmental effects.

We calculate Bayes factors to compare the evidence for the correct models that include the environmental effects, versus vacuum. The Bayes factor is defined as the ratio of the evidence $p(d|D)$ for a signal d under two different models (here A and B):

$$\mathcal{B}(d) = \frac{p(d|A)}{p(d|B)}. \tag{7}$$

For a model A with parameters θ, the evidence is defined as

$$p(d|A) = \int {\rm d}\theta\, p(d|h_\theta)\, p(\theta), \tag{8}$$

where $p(\theta)$ is the prior on the model parameters, $h_\theta(t)$ is the waveform corresponding to parameters θ and $p(d|h_\theta)$ is the likelihood describing how probable the data are under that waveform model. We can extract an estimate for the evidence using nested sampling. We find $\log_{10}\mathcal{B} = 34$ for the dark dress, $\log_{10}\mathcal{B} = 6$ for the accretion disk and $\log_{10}\mathcal{B} = 39$ for the gravitational atom, demonstrating undeniable support for the correct model in each case, even though there are clean posteriors for the chirp mass with a vacuum template in each case. Systems with parameter values that lead to higher SNR loss with respect to vacuum will lead to even larger Bayes factors, and it is unlikely that such systems will be detectable at all by matched filtering searches using only vacuum templates.

Finally, we ascertain whether we can distinguish between environments by computing the Bayes factors to compare each non-vacuum environment with every other one. We compute these Bayes factors for the same benchmark systems. The results are summarized in Table 2.

The Bayes factors are very large, orders of magnitude larger than the $\mathcal{B} \sim \mathcal{O}(100)$ threshold for 'confident' Bayesian preference for one model over another[50,51]. This shows that we can confidently distinguish

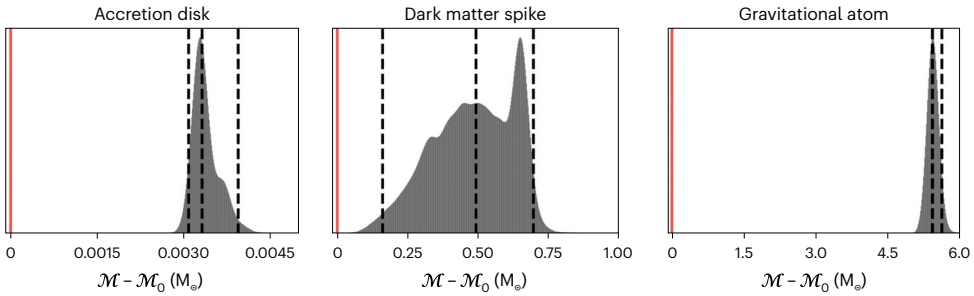

Fig. 4 | Parameter estimation using a vacuum template. Posterior distribution for the chirp mass of an accretion disk (left), dark matter spike (middle) and gravitational atom (right) signals when fitted with a vacuum template, all with 1 year duration. The true chirp mass, $\mathcal{M}_0$, is indicated by the red vertical line at $\mathcal{M} - \mathcal{M}_0 = 0$. The outermost black dashed vertical lines show the 95% credible intervals of the posteriors and the central dashed black line is the median value of the posteriors.

Table 2 | Logarithm of the Bayes factors, $\log_{10}\mathcal{B}$, comparing the evidence for the correct template that fits the signal versus an incorrect template

	Dark dress signal	Accretion disk signal	Gravitational atom signal
Vacuum template	34	6	39
Dark dress template	—	3	39
Accretion disk template	17	—	33
Gravitational atom template	24	6	—

between environments when we compare the evidence for the parameter inference on a given signal with each environmental template bank. While the environmental templates can mimic each other to a certain extent (in most cases better than the vacuum template; Supplementary Information), the driving force for the distinguishability is the way that the environments' waveforms evolve as a function of time, which makes it difficult to fit the waveform of one environment by varying the parameters of another.

We estimate by how much these Bayes factors will degrade with systematic uncertainties on the template waveforms by re-calculating the evidence for the correct template with a multiplicative factor on the phase of the signal. This means that the template bank for the correct environmental model no longer contains exactly the signal owing to the offset in the phase that we added by hand. We compare the evidence for the offset signal with the correct and incorrect environmental model template banks that we used before, and calculate these Bayes factors. In this case, the overall phase scaling of the dark dress system should be known to better than 0.1% precision in order to confidently distinguish the system from other environments (that is, a Bayes factor greater than 100), while for the gravitational atom, the phase scaling should be known to better than 0.01% precision. For the accretion disk, since we fix the mass ratio and therefore it is difficult for the other two parameter values to mimic a shift in the phase, the signal waveform needs to be completely contained within the template bank in order to achieve the Bayes factors in Table 2.

Furthermore, performing parameter inference including the extrinsic parameters, as well as using post-Newtonian waveforms that include spins and eccentricity that are not present in our analysis, will also probably decrease the Bayes factors. However, we emphasize that the relative difference in the Bayes factors is large and that we can confidently distinguish between environments on this basis.

Conclusions

Measuring the properties of the environments of IMRIs will be possible with next-generation GW detectors. We have demonstrated that we can accurately reconstruct the parameters describing DM spikes, accretion disks and gravitational atoms around an intermediate mass BH, given a signal detected with an SNR of 15 of 1 year's duration. We have also shown that we can confidently distinguish between environments by comparing the Bayesian evidence for using the correct environmental template for a given signal with an incorrect one. The correct environmental template is always strongly preferred, showing that we will not be at risk of misinterpreting an environmental signal for either a biased vacuum system, or the wrong type of environment. Furthermore, we show that SNR losses can be substantial if the wrong template is used to fit the signal, and we therefore conclude that it is vital that environmental effects be taken into account when searching for and analysing long-duration signals from future GW detectors.

This work serves as a proof of concept for distinguishing between environments and as a starting point for future refinements. In particular, a more complex analysis will require waveforms that take into account relativistic effects[52], and a detailed study of possible degeneracies between environmental effects and post-Newtonian effects[53], transient orbital resonances[54], modified gravity, as well as eccentricity[39,55] and effects related to the spins of the BHs[56]. Finally, realistic data analysis strategies will need to be developed to deal with the new challenges that long duration signals will demand. This will include removing tens of thousands of galactic binaries[57,58] in order to extract clean IMRI/EMRI signals as well as coping with gaps in the data[59,60].

Data availability

No raw data were used in the completion of this manuscript.

Code availability

`HaloFeedback` code can be accessed at ref. 61. `pydd` code can be accessed at https://github.com/adam-coogan/pydd. For specific adaptations of these codes made for this manuscript, please email p.s.cole@uva.nl.

References

1. Baker, J. et al. The Laser Interferometer Space Antenna: Unveiling the Millihertz Gravitational Wave Sky. https://doi.org/10.48550/arXiv.1907.06482 (2019).
2. Luo, Z., Wang, Y., Wu, Y., Hu, W. & Jin, G. The Taiji program: a concise overview. *Prog. Theor. Exp. Phys.* **2021**, 05A108 (2021).
3. Kawamura, S. et al. Current status of space gravitational wave antenna DECIGO and B-DECIGO. *Prog. Theor. Exp. Phys.* **2021**, 05A105 (2021).
4. Luo, J. et al. TianQin: a space-borne gravitational wave detector. *Class. Quant. Grav.* **33**, 035010 (2016).
5. Aasi, J. et al. Advanced LIGO. *Class. Quant. Grav.* **32**, 074001 (2015).

6. Acernese, F. et al. Advanced Virgo: a second-generation interferometric gravitational wave detector. *Class. Quant. Grav.* **32**, 024001 (2015).
7. Akutsu, T. et al. Overview of KAGRA: detector design and construction history. *Prog. Theor. Exp. Phys.* **2021**, 05A101 (2021).
8. Macedo, C. F. B., Pani, P., Cardoso, V. & Crispino, L. C. B. Into the lair: gravitational-wave signatures of dark matter. *Astrophys. J.* **774**, 48 (2013).
9. Barausse, E., Cardoso, V. & Pani, P. Can environmental effects spoil precision gravitational-wave astrophysics? *Phys. Rev. D* **89**, 104059 (2014).
10. Barausse, E., Cardoso, V. & Pani, P. Environmental effects for gravitational-wave astrophysics. *J. Phys. Conf. Ser.* **610**, 012044 (2015).
11. Berry, C. et al. The unique potential of extreme mass-ratio inspirals for gravitational-wave astronomy. *Bull. Am. Astron. Soc.* **51**, 42 (2019).
12. Tanaka, H., Takeuchi, T. & Ward, W. R. Three-dimensional interaction between a planet and an isothermal gaseous disk. I. Corotation and Lindblad torques and planet migration. *Astrophys. J.* **565**, 1257–1274 (2002).
13. Derdzinski, A. M., D'Orazio, D., Duffell, P., Haiman, Z. & MacFadyen, A. Probing gas disc physics with LISA: simulations of an intermediate mass ratio inspiral in an accretion disc. *Mon. Not. Roy. Astron. Soc.* **486**, 2754–2765 (2019). [Erratum: Mon. Not. R. Astron. Soc. **489**, 4860–4861 (2019)].
14. Duffell, P. C. et al. Circumbinary disks: accretion and torque as a function of mass ratio and disk viscosity. *Astrophys. J.* **901**, 25 (2020).
15. Derdzinski, A., D'Orazio, D., Duffell, P., Haiman, Z. & MacFadyen, A. Evolution of gas disc–embedded intermediate mass ratio inspirals in the LISA band. *Mon. Not. R. Astron. Soc.* **501**, 3540–3557 (2020).
16. Speri, L. et al. Measuring accretion-disk effects with gravitational waves from extreme mass ratio inspirals. Preprint at https://arxiv.org/abs/2207.10086 (2022).
17. Yunes, N., Kocsis, B., Loeb, A. & Haiman, Z. Imprint of accretion disk-induced migration on gravitational waves from extreme mass ratio inspirals. *Phys. Rev. Lett.* **107**, 171103 (2011).
18. Kocsis, B., Yunes, N. & Loeb, A. Observable signatures of extreme mass-ratio inspiral black hole binaries embedded in thin accretion disks. *Phys. Rev. D* **84**, 024032 (2011).
19. Gondolo, P. & Silk, J. Dark matter annihilation at the galactic center. *Phys. Rev. Lett.* **83**, 1719–1722 (1999).
20. Bertone, G., Zentner, A. R. & Silk, J. A new signature of dark matter annihilations: gamma-rays from intermediate-mass black holes. *Phys. Rev. D* **72**, 103517 (2005).
21. Eda, K., Itoh, Y., Kuroyanagi, S. & Silk, J. New probe of dark-matter properties: gravitational waves from an intermediate-mass black hole embedded in a dark-matter minispike. *Phys. Rev. Lett.* **110**, 221101 (2013).
22. Eda, K., Itoh, Y., Kuroyanagi, S. & Silk, J. Gravitational waves as a probe of dark matter minispikes. *Phys. Rev. D* **91**, 044045 (2015).
23. Yue, X.-J., Han, W.-B. & Chen, X. Dark matter: an efficient catalyst for intermediate-mass-ratio-inspiral events. *Astrophys. J.* **874**, 34 (2019).
24. Kavanagh, B. J., Nichols, D. A., Bertone, G. & Gaggero, D. Detecting dark matter around black holes with gravitational waves: effects of dark-matter dynamics on the gravitational waveform. *Phys. Rev. D* **102**, 083006 (2020).
25. Coogan, A., Bertone, G., Gaggero, D., Kavanagh, B. J. & Nichols, D. A. Measuring the dark matter environments of black hole binaries with gravitational waves. *Phys. Rev. D* **105**, 043009 (2022).
26. Dai, N., Gong, Y., Jiang, T. & Liang, D. Intermediate mass-ratio inspirals with dark matter minispikes. *Phys. Rev. D* **106**, 064003 (2022).
27. Hannuksela, O. A., Ng, K. C. Y. & Li, T. G. F. Extreme dark matter tests with extreme mass ratio inspirals. *Phys. Rev. D* **102**, 103022 (2020).
28. Dolan, S. R. Instability of the massive Klein–Gordon field on the Kerr spacetime. *Phys. Rev. D* **76**, 084001 (2007).
29. Arvanitaki, A., Dimopoulos, S., Dubovsky, S., Kaloper, N. & March-Russell, J. String axiverse. *Phys. Rev. D* **81**, 123530 (2010).
30. Arvanitaki, A. & Dubovsky, S. Exploring the string axiverse with precision black hole physics. *Phys. Rev. D* **83**, 044026 (2011).
31. Brito, R., Cardoso, V. & Pani, P. Superradiance. *Lect. Notes Phys.* **906**, 1–237 (2015).
32. Baumann, D., Chia, H. S., Stout, J. & ter Haar, L. The spectra of gravitational atoms. *J. Cosmol. Astropart. Phys.* **12**, 006 (2019).
33. Baumann, D., Chia, H. S., Porto, R. A. & Stout, J. Gravitational collider physics. *Phys. Rev. D* **101**, 083019 (2020).
34. Baumann, D., Bertone, G., Stout, J. & Tomaselli, G. M. Ionization of gravitational atoms. *Phys. Rev. D* **105**, 115036 (2022).
35. Baumann, D., Bertone, G., Stout, J. & Tomaselli, G. M. Sharp signals of boson clouds in black hole binary inspirals. *Phys. Rev. Lett.* **128**, 221102 (2022).
36. Yoshino, H. & Kodama, H. Gravitational radiation from an axion cloud around a black hole: superradiant phase. *Prog. Theor. Exp. Phys.* **2014**, 043E02 (2014).
37. Shakura, N. I. & Sunyaev, R. A. Black holes in binary systems. Observational appearance. *Astron. Astrophys.* **24**, 337–355 (1973).
38. McKernan, B., Ford, K. E. S., Lyra, W. & Perets, H. B. Intermediate mass black holes in AGN discs - I. production and growth. *Mon. Not. R. Astron. Soc.* **425**, 460–469 (2012).
39. Becker, N., Sagunski, L., Prinz, L. & Rastgoo, S. Circularization versus eccentrification in intermediate mass ratio inspirals inside dark matter spikes. *Phys. Rev. D* **105**, 063029 (2022).
40. Binney, J. & Tremaine, S. *Galactic Dynamics, 2nd edn* (Princeton University Press, 2008).
41. Goldreich, P. & Tremaine, S. The excitation of density waves at the Lindblad and corotation resonances by an external potential. *Astrophys. J.* **233**, 857–871 (1979).
42. Gair, J. R. et al. Event rate estimates for LISA extreme mass ratio capture sources. *Class. Quant. Gravity* **21**, S1595–S1606 (2004).
43. Greene, J. E., Strader, J. & Ho, L. C. Intermediate-mass black holes. *Annu. Rev. Astron. Astrophys.* **58**, 257–312 (2020).
44. Hannuksela, O. A., Wong, K. W. K., Brito, R., Berti, E. & Li, T. G. F. Probing the existence of ultralight bosons with a single gravitational-wave measurement. *Nat. Astron.* **3**, 447–451 (2019).
45. Jiang, J. et al. High density reflection spectroscopy – II. The density of the inner black hole accretion disc in AGN. *Mon. Not. R. Astron. Soc.* **489**, 3436–3455 (2019).
46. Skilling, J. Nested Sampling. In *Bayesian Inference and Maximum Entropy Methods in Science and Engineering* (eds. Fischer, R., Preuss, R. & von Toussaint, U.) 395–405 (American Institute of Physics, 2004).
47. Skilling, J. Nested sampling for general Bayesian computation. *Bayesian Anal.* **1**, 833–859 (2006).
48. Feroz, F., Hobson, M. P. & Bridges, M. MULTINEST: an efficient and robust Bayesian inference tool for cosmology and particle physics. *Mon. Not. R. Astron. Soc.* **398**, 1601–1614 (2009).
49. Speagle, J. S. DYNESTY: a dynamic nested sampling package for estimating Bayesian posteriors and evidences. *Mon. Not. R. Astron. Soc.* **493**, 3132–3158 (2020).
50. Jeffreys, H. *The Theory of Probability* (Oxford Univ. Press, 1998).
51. Kass, R. E. & Raftery, A. E. Bayes factors. *J. Am. Stat. Assoc.* **90**, 773–795 (1995).
52. Cardoso, V., Destounis, K., Duque, F., Macedo, R. P. & Maselli, A. Gravitational waves from extreme-mass-ratio systems in astrophysical environments. *Phys. Rev. Lett.* **129**, 241103 (2022).

53. Speeney, N., Antonelli, A., Baibhav, V. & Berti, E. Impact of relativistic corrections on the detectability of dark-matter spikes with gravitational waves. *Phys. Rev. D* **106**, 044027 (2022).
54. Speri, L. & Gair, J. R. Assessing the impact of transient orbital resonances. *Phys. Rev. D* **103**, 124032 (2021).
55. Yue, X.-J. & Cao, Z. Dark matter minispike: a significant enhancement of eccentricity for intermediate-mass-ratio inspirals. *Phys. Rev. D* **100**, 043013 (2019).
56. Fairhurst, S., Green, R., Hannam, M. & Hoy, C. When will we observe binary black holes precessing? *Phys. Rev. D* **102**, 041302 (2020).
57. Zhang, X.-H., Mohanty, S. D., Zou, X.-B. & Liu, Y.-X. Resolving galactic binaries in LISA data using particle swarm optimization and cross-validation. *Phys. Rev. D* **104**, 024023 (2021).
58. Strub, S. H., Ferraioli, L., Schmelzbach, C., Stähler, S. C. & Giardini, D. Bayesian parameter estimation of galactic binaries in LISA data with Gaussian process regression. *Phys. Rev. D* **106**, 062003 (2022).
59. Baghi, Q. et al. Gravitational-wave parameter estimation with gaps in LISA: a Bayesian data augmentation method. *Phys. Rev. D* **100**, 022003 (2019).
60. Dey, K. et al. Effect of data gaps on the detectability and parameter estimation of massive black hole binaries with lisa. *Phys. Rev. D* **104**, 044035 (2021).
61. Kavanagh, B. J. HaloFeedback code version 0.9. *GitHub* https://github.com/bradkav/HaloFeedback (2020).

Acknowledgements

We thank P. Pani and S. Witte for helpful discussions. P.S.C. acknowledges support from the Institute of Physics at the University of Amsterdam. A.C. received funding from the Schmidt Futures Foundation. D.G. was supported by Spanish MINECO through the Ramon y Cajal programme RYC2020-029184-I between September 2022 and November 2022 and is currently supported from the project 'Theoretical Astroparticle Physics (TAsP)' funded by the National Institute for Nuclear Physics (INFN). B.J.K. thanks the Spanish Agencia Estatal de Investigación (AEI, Ministerio de Ciencia, Innovación y Universidades) for the support to the Unidad de Excelencia María de Maeztu Instituto de Física de Cantabria (ref. MDM-2017-0765). T.F.M.S. is supported by VILLUM FONDEN (grant no. 37766), the Danish Research Foundation and the European Union's H2020 ERC Advanced Grant 'Black holes: gravitational engines of discovery' (grant agreement no. Gravitas-101052587).

Author contributions

P.S.C. conducted the main analysis in this manuscript and produced all of the figures. G.B. initiated the project idea and coordinated the members of the group. A.C. provided the dark dress code for the analysis that was extended for use in this broader context. D.G. consulted on issues to do with DF and gas torques. T.K. wrote the surrogate model and did the analysis for the dark dress that appears in the Supplementary Information. B.J.K. provided code for calculating feedback processes. T.F.M.S. and G.M.T. provided code for calculating the energy losses for the gravitational atom. All authors contributed to writing and editing the manuscript.

Competing interests

The authors declare no competing interests.

Additional information

Supplementary information The online version contains supplementary material available at https://doi.org/10.1038/s41550-023-01990-2.

Correspondence and requests for materials should be addressed to Philippa S. Cole.

Peer review information *Nature Astronomy* thanks the anonymous reviewers for their contribution to the peer review of this work.